

COSMIC RAY NUCLEI MEASUREMENTS IN SPACE WITH NINA EXPERIMENT

A. Morselli, R.Sparvoli on the behalf of NINA Collaboration
Dept. of Physics, II Univ. of Rome "Tor Vergata" and INFN, Italy

Abstract

In June 1998 the telescope NINA has been launched in space on board of the Russian satellite Resource-01 n.4. The main scientific objective of the mission is the study of the Anomalous, Galactic and Solar components of the Cosmic Rays in the energy interval 10-200 MeV/n.

0.1 Introduction: the detector

The active part of the NINA instrument is a telescope composed of 16 X-Y planes, giving information on the energy of the crossing particle and its incident angle. The sensitive element consists of two n-type silicon detectors, 60×60 mm², each divided in 16 strips and attached to a supporting ceramic frame passing under the lateral strips 1 and 16. The couple of detectors is mounted with the strips right-angled, in order to measure the X and Y coordinates of the detected particle. The thickness of the first two detectors is 150 ± 15 μ m; all the others, instead, are 380 ± 15 μ m thick, so to have 11.7 silicon mm in total [2].

The lateral strips (n.1 and n.16) are used for the anticoincidence system (AC) and are read together by the same electronic channel, except for the plane 1 where they are physically disconnected. The planes are vertically stacked; interplanar distance is 1.4 cm, except for the first and second planes separated by 8.5 cm, for a better measurement of the particle incident angle. The 16 planes are modular, so that mechanically and electronically they are interchangeable. Below the 16 active modules, other 4 cards are placed, dedicated to the trigger electronics, silicon power supply, analog-digital conversion, FIFO.

The geometrical factor is 8.3 cm²sr for low energy particles which stop in the second plane, and it decreases with growing energy.

The whole structure is surrounded by an aluminum vessel, a cylinder of 284 mm diameter and 480 mm height. The vessel is 2 mm thick, apart from a little window in correspondence to the first silicon plane where it is reduced to 300 μm ; this choice has been made so to decrease the amount of passive material the particles cross before reaching the sensitive detector.

The signal produced by the incoming particles in the silicon strips has to be amplified and shaped before performing the conversion from analog to digital. Each plane of the telescope has two 16 channels preamplifiers.

The analogic signal is digitized by a 12 bit (4096 channels) ADC. The ADC overflow channel corresponds to 2800 mip, where 1 mip in 380 μm of silicon is equivalent to 30400 electrons or 105 keV; the resolution per channel is about 0.68 mip/ch, or 0.07 MeV/ch.

0.2 Operating conditions

NINA can work in different operating conditions, switched automatically or via telecommand, and affecting the trigger system. In particular:

1. Two thresholds for the energy deposits in the single silicon layers have been implemented: a *Low Threshold* (L.T.), corresponding to 2.5 mips, and a *High Threshold* (H.T.), corresponding to 25 mips.

In the first two layers, in order to compensate the smaller thickness, the High Threshold corresponds to 0.4 of the one previously defined.

2. The strips 1 and 16 of every silicon layer are used as Lateral Anticoincidence system, and are physically connected to the same output.
3. The planes 15 and 16 can be used as Bottom Anticoincidence. The usual operating mode adopts the plane 16 but, in case of failure, the plane 15 can be selected by telecommand.

The basic operating trigger of the acquisition system is the following:

$$TRGM1 = D_{1x} \times D_{1y} \times ((D_{2x} + D_{2y}) + (D_{3x} + D_{3y})) \times \\ \times \overline{D_{16x}} \times \overline{D_{16y}} \times \overline{LAT},$$

where D_{ij} is the above-threshold signal coming from the plane i , view j ($j=x,y$), and LAT is the logic OR of all signals coming from the strips defining the Lateral Anticoincidence. The logic OR of planes 2 and 3 provides redundancy in case of a failure of plane 2.

Particle	Z	E_{min} (MeV/n) TRG M1	E_{max} (MeV/n)	E_{min} (MeV/n) TRG M2
1H	1	10.0	48.0	18
2H	1	6.5	32.0	12.5
3H	1	5.0	25.3	9.7
3He	2	11.0	55.7	21.3
4He	2	9.25	47.2	18.0
6Li	3	11.5	59.3	22.7
7Li	3	10.6	54.4	20.7
7Be	4	14.6	75.1	28.6
9Be	4	12.7	65.2	24.8
^{10}B	5	16.0	79.0	31.0
^{11}B	5	14.6	74.6	29.1
^{12}C	6	17.5	87.5	33.3
^{14}N	7	18.6	95.0	36.4
^{16}O	8	20.0	103.1	39.4
^{19}F	9	21.0	106.8	40.5
^{20}Ne	10	23.0	117.0	44.5
^{28}Si	14	27.5	141.8	53.6
^{40}Ca	20	38.5	174.5	65.3
^{56}Fe	26	58.2	194.6	72.5

Table 1: Energy windows for the most abundant particles in NINA detector. Column 3: E_{min} using TRG M1; Column 5: E_{min} using TRG M2.

This trigger can be used with Low or a High Threshold, defining two different intervals of atomic numbers for nuclei. In particular TRG M1, together with High Threshold, cuts from the trigger all protons and a very small percentage of heliums (figure 1). Finally, TRG M1 allows a good reconstruction of the particle trajectory. For particular data taking demands, or in case of failure of the first plane, it is possible to switch, via telecommand, to a second trigger logic:

$$TRG\ M2 = (D_{2x} + D_{2y}) \times (D_{3x} + D_{3y}) \times (D_{4x} + D_{4y}) \times (D_{5x} + D_{5y}) \times \\ \times \overline{D_{16x}} \times \overline{D_{16y}} \times \overline{LAT}.$$

This trigger increases the acceptance angle, although with a worsening of the angular resolution. The combination of TRG M2 and High Threshold excludes most of the protons from the trigger (which are in much higher percentage and fill the storage memory very quickly), but keeps all He nuclei.

The acceptance window for Low Threshold acquisition and both TRG M1 and TRG M2 is shown in table 1. The spectrum of particles extends from hydrogen to iron, and the energy window in the interval 10 - 200 MeV/n.

0.3 Acquisition modes

The maximum amount of data that NINA can send to ground from the satellite varies between 2 and 4 Mbyte/day, out of a total mass memory of 14 Mbytes. Therefore, a limit to the acquisition capability of the instrument has been provided, organizing a system which, at high rate conditions, enables the detector to register events with less detail.

The flux of particles changes notably along the orbit, so that three data acquisition and storage modes have been foreseen, depending on the counting rate:

Full-Format mode (counting rate up to 10 Hz). This mode, in which the whole event topology is recorded, is the normal working configuration outside the Earth Radiation Belts. It allows to measure the energy released by the particle in each silicon detector (Bragg curve). Within the precision allowed by the strip pitch, we can also reconstruct the particle trajectory, identify its range with good precision and check for multiple tracks and for particles escaping the telescope, due to the geometrical inefficiencies of the anticoincidence system.

E_1 - E_{tot} mode (counting rate 10-100 Hz). At high fluxes, to make an optimal use of the mass memory storage, the total energies released in the first plane (E_1) and in the whole detector (E_{tot}) by the crossing particle are calculated. Moreover, to select mainly single and not escaping tracks, a Second Level trigger restricts the event acceptance only to particles crossing the 4 central strips of the first 2 planes of the telescope, and leaving a single cluster of fired strips (multiple tracks subtraction). Once these conditions have been fulfilled, only the E_1 and E_{tot} information of the event are transmitted.

Rate Meter mode (counting rate above 100 Hz). If the trigger rate rises above 100 Hz, only the counting rates of some planes, chosen at different depths of the telescope, are read and stored every 6 minutes. Two signal integration systems have been implemented, so to have information both at high and low rates.

The scientific information in Rate Meter mode is obviously strictly reduced, but still allows to have a global check of the system and an estimation of the rate of particles inside the Radiation Belts or in presence

of solar flares.

The switching among the different acquisition modes is instantaneous. In order to avoid oscillations between the modes, which could bring to a fragmented scientific information, every passage between one state and the next can happen only at minimum intervals of 60 seconds.

0.4 Energy calibration

The detector has been calibrated by comparing the energy deposits of the collected families of nuclei, from proton to carbon, expressed in ADC channels, with the corresponding simulated ones expressed in MeV. Montecarlo simulation programs had been previously calibrated by using monocromatic proton and helium beams at the PSI Laboratory of Willigen (Zurich - Switzerland).

Figure 2 shows some Bragg curves for carbon experimental data. The tracks chosen for the calibration were straight, clean, without double or missing signals, and right in the central strips of the detector.

The average ratio between MeV energy and ADC channels obtained from the data is the following:

$$R = (0.067 \pm 0.002) \frac{MeV}{ADC Ch} . \quad (1)$$

Figure 3 shows the E_1 vs E_{tot} curves of real particles, coming from the fragmentation of the original carbon beam by means of the polyethylene target, with energies expressed in MeV. All the products of fragmentation are visible, and the energy behavior is in perfect agreement with the expected simulated data [1].

0.5 Mass analysis

The *Full-Format* acquisition mode allows the complete registration of the track of the particle with all its energy deposits in the strips and therefore, in this condition, the best nuclear and isotope discrimination can be performed.

Figure 3 shows how the nuclear families coming from the fragmentation of the ^{12}C beam are well separated by the simple E_1 vs E_{tot} technique. Nevertheless, we can better identify groups of equal Z number by using a well tuned product of the E_1 and E_{tot} deposits. The product $E_1 \times E_{tot}$ is an effective tool for identifying groups of equal atomic number Z , as can be seen in figure 4.

Once the charge has been identified, the masses M of the different isotopes can be reconstructed by means of the equation:

$$M = \left(\frac{a(E^b - (E - \Delta E)^b)}{Z^2 \Delta x} \right)^{\frac{1}{b-1}}, \quad (2)$$

where ΔE is the energy lost by the particle in an optimized thickness Δx measured starting from the first plane. This algorithm of mass reconstruction is well known in literature [3] and adopted in many experiments [4].

The parameter a is a constant of the medium and the parameter b has a value between 1.5 and 1.8 in NINA's energy range. A precise evaluation of such parameters for each particle has been obtained by a fit of the following expression:

$$R = a \frac{M}{Z^2} \left(\frac{E}{M} \right)^b, \quad (3)$$

where R and E are respectively the measured range and kinetic energy of known particles of mass M and charge Z . The procedure of fitting has been done for GSI and simulated data, and the two sets of a and b parameters have shown a perfect agreement.

The incident direction of the particle must be taken into account. For a particle impinging with angles θ_x and θ_y and hitting n (n_x and n_y) views, the expression for Δx will be:

$$\begin{aligned} \Delta x = & (150\mu m + (n_x^{\Delta x} - 1)380\mu m)/\cos\theta_x + \\ & +(150\mu m + (n_y^{\Delta x} - 1)380\mu m)/\cos\theta_y, \end{aligned} \quad (4)$$

where $n_x^{\Delta x}$ and $n_y^{\Delta x}$ are respectively the number of X and Y views composing Δx . 150 μm is the contribution of the first two thin silicon detectors and the rest is the contribution of all the normal 380 μm thick silicon views.

Z	Isotope, $M(\text{MeV})$	\overline{M} (MeV)	σ (MeV)	σ (amu)
1	^1H , 938	939	67	0.072
1	^2H , 1875	1834	153	0.164
1	^3H , 2814	2761	191	0.205
2	^3He , 2814	2828	146	0.157
2	^4He , 3727	3742	155	0.167
3	^6Li , 5603	5589	154	0.165
3	^7Li , 6535	6545	208	0.223
4	^7Be , 6536	6504	214	0.230
4	^9Be , 8394	8409	237	0.254
4	^{10}Be , 9328	9359	206	0.222
5	^{10}B , 9327	9278	282	0.303
5	^{11}B , 10255	10170	290	0.311
6	^{12}C , 11178	11239	279	0.300

Table 2: Medium averages M and sigmas σ from the Gaussian fits of the masses reconstructed by eq. 2, for real events collected at GSI.

Starting from $Z=1$ till $Z=6$, we reconstructed all isotope masses, as shown in figures 5 and 6. For every mass, a Gaussian fit has been performed, evaluating in such a way the average value of the reconstructed mass M and its corresponding sigma σ . The results of this analysis are resumed in table 2, for all isotopes studied. As it can be seen by the pictures and the table, the sigmas of the reconstructed masses become wider increasing the nuclear charge Z .

Results up to carbon give sigmas of about 0.3 amu. Such results confirm the good capability of this instrument to perform isotope analysis.

References

- [1] A. Bakaldin, et al. - *Astroparticle Physics* 8 (1997), 109.
- [2] R. Bellotti, et al. - *Astroparticle Physics* 7 (1997), 219.
- [3] F. S. Goulding - *NIM* 162 (1979), 609.
- [4] D. N. Baker, et al. - *IEEE Trans. on Geoscience and Remote Sensing* 31-3 (1993), 531.

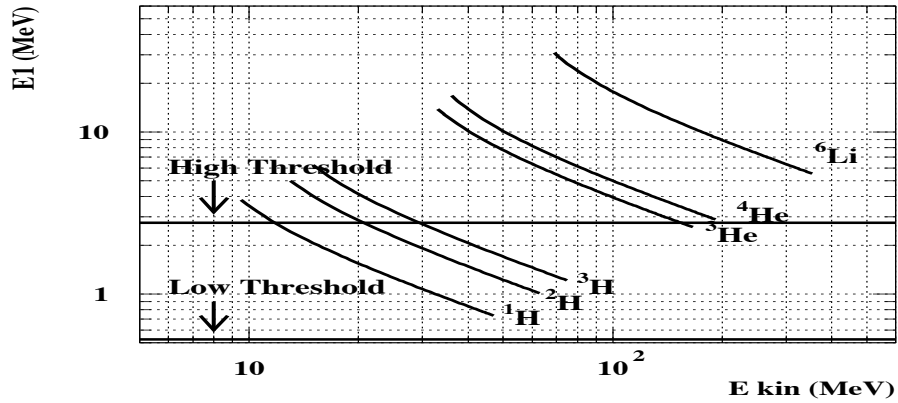


Figure 1: Effects of the High and Low Threshold on the acquisition of 1H , 2H , 3H , 3He , 4He e 6Li contained in the detector, in case of TRG M1.

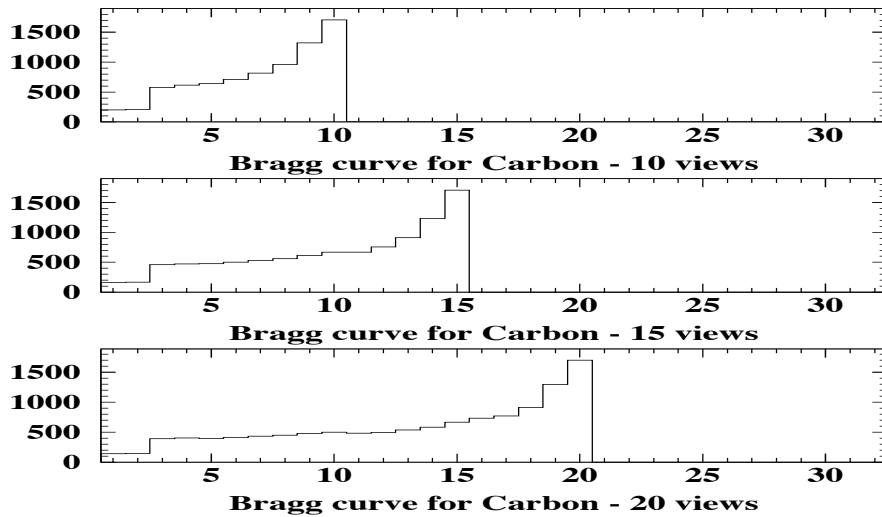


Figure 2: Bragg curves for real carbons at different ranges. X axis: n. of views in the detector ($1 < n < 32$); Y axis: energy deposit in ADC channels.

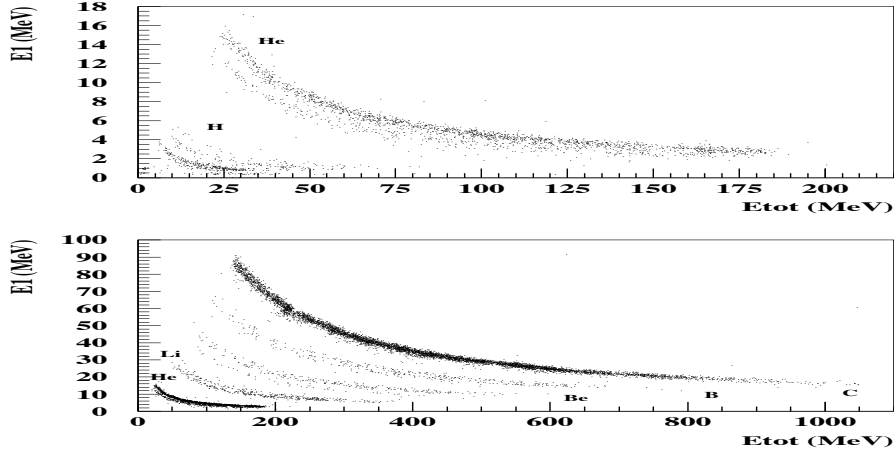


Figure 3: Distribution of the energy released in the first plane (E_1) versus the energy released in the whole detector (E_{tot}) for real particles coming from fragmentation of ^{12}C , produced at GSI.

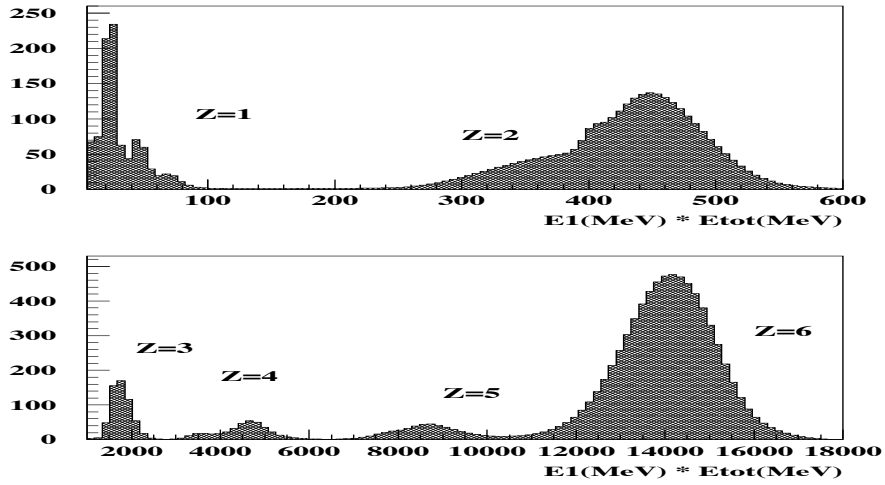


Figure 4: Distribution of the energy released in the first plane (E_1) multiplied by the energy released in the whole detector (E_{tot}) for real particles coming from fragmentation of ^{12}C , produced at GSI.

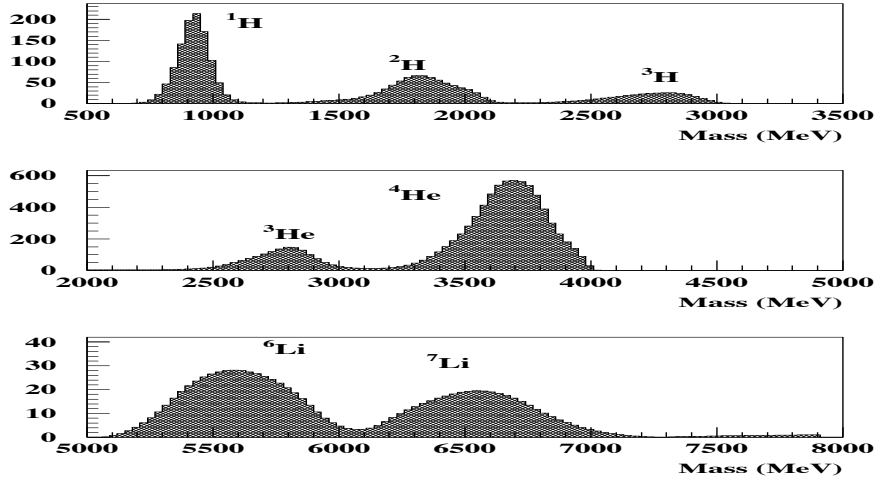


Figure 5: Distributions of the masses reconstructed by eq. 2 for real events of $Z = 1$, $Z = 2$ e $Z = 3$. N. of events on Y axis.

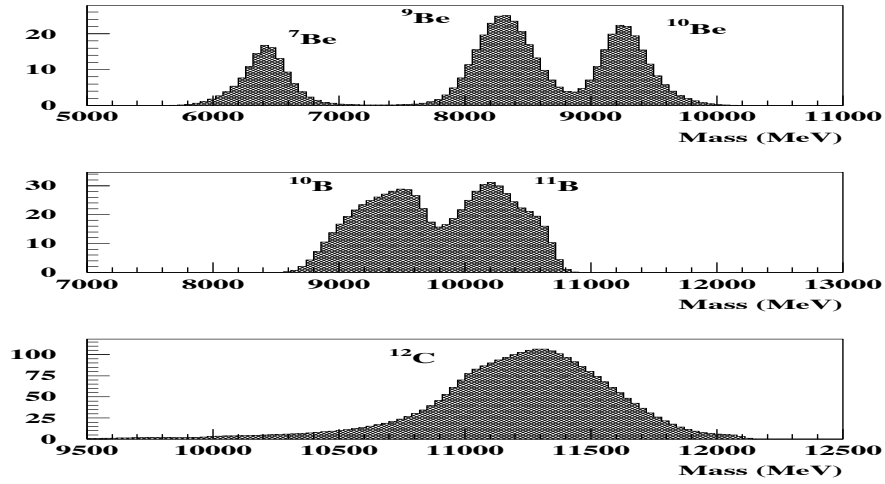


Figure 6: Distributions of the masses reconstructed by eq. 2 for real events of $Z = 4$, $Z = 5$ e $Z = 6$. N. of events on Y axis.